

Material sensitivity and formability prediction of warm-forming magnesium alloy sheets with experimental verification

L. C. Chan · X. Z. Lu

Received: 7 May 2013 / Accepted: 15 October 2013 / Published online: 23 November 2013
© Springer-Verlag London 2013

Abstract This paper proposes a theoretical method for predicting the formability of magnesium alloy sheets at elevated temperatures by combining the Marciniak and Kuczinsky model with the Logan–Hosford yield criterion. In addition, the material sensitivity under different strain rates from 0.001 to 0.1 s⁻¹ and elevated temperatures on forming the magnesium alloy was also investigated in this study. Forming limit tests on AZ31B magnesium alloy sheets were performed concurrently for the theoretical forming limit diagram (FLD) verification using a self-developed forming facility at elevated temperatures of 200, 250, and 300 °C and, simultaneously, the material sensitivity effect under a selective strain rate of 0.01 s⁻¹. Based on the verified FLD prediction results, numerical simulations of warm-forming a AZ31B camera casing of thickness 0.8 mm as an example were then carried out. The warm forming experiments for this camera casing, under the identical conditions, were also performed for verification. As a consequence, it was found that the effect of strain rate on the prediction of FLDs did have a significant influence with increasing temperatures. Furthermore, the results of numerical simulations showed a good agreement with those of the warm forming experiments at different elevated temperatures. The proposed theoretical method offers a relatively accurate prediction in warm-forming magnesium alloy sheets and should lead to a remarkable reduction of trials, at least in the sense of both time and cost benefits, before a large batch production. Such outcomes of the study are expected to

be very helpful and contributive to professionals, engineers, and the magnesium alloy-related applications in industry.

Keywords Magnesium alloy · Forming limit diagrams · Marciniak and Kuczinsky model · Warm forming

1 Introduction

Presently, magnesium alloy parts are used widely in many structural components due to the light weight and high specific strength of magnesium [1, 2]. However, the magnesium alloy has poor formability at room temperature due to the close-packed hexagonal structure of magnesium. Therefore, the warm forming process has been developed to improve the formability of magnesium alloy sheets [3]. It has been reported that the formability of AZ31B magnesium alloy sheets can be improved significantly at elevated temperatures between 200 and 300 °C [4–7]. Therefore, the warm forming process of AZ31B sheets at elevated temperatures has been investigated by many scholars [8–13].

In the magnesium alloy sheet forming process, the accurate prediction of sheet metal formability plays a pivotal role. A predominant method of estimating the sheet metal formability is the forming limit diagram (FLD) introduced by Keeler and Backofen [14]. The FLD provides information on the maximum strain the sheet metal can undergo before fracturing or necking. The diagrams are constructed by using test strips of sheet metal and measuring the deformation. However, the determination of FLD is a complex task; therefore, a series of tests, together with extensive theoretical studies, should be addressed [15].

A lot of earlier research has explored plastic instability in the sheet metal forming process and the determination of FLD. Swift proposed a criterion for predicting the onset of diffuse necking with the assumption that plastic instability

L. C. Chan (✉) · X. Z. Lu
Department of Industrial and Systems Engineering, The Hong Kong Polytechnic University, Hung Hom, Kowloon, Hong Kong S.A.R., China
e-mail: lc.chan@polyu.edu.hk

X. Z. Lu
e-mail: mfxz.lu@connect.polyu.hk

occurs at a maximum load [16]. Hill developed a localized necking method [17]; this method assumes that the necking band develops normally to the direction of the zero extension in a sheet metal. Marciniak and Kuckzinsky introduced the groove hypothesis into sheet metals, based on which a localized necking takes place. This method is the well-known Marciniak and Kuckzinsky (M–K) theory [18]. The inhomogeneity of physical property or thickness can be caused by factors such as local grain size variation, alloys elements, or texture. Hutchinson and Neale [19] extended the M–K theory based on a J2 deformation theory. Therefore, both the positive strain ratio and negative strain ratio can be calculated by M–K analysis. Due to the clear physical significance and simple mathematical formula, the M–K theory has been employed widely. The implementation of different yield criteria in the M–K model have been investigated by several authors [20–23]. In this study, a yield criterion proposed by Logan–Hosford was employed since it can describe well the magnesium alloy sheet yield surface at high temperatures [24].

In this paper, the theoretical computation of FLD (M–K model+Logan–Hosford yield criterion) is addressed in Section 2. Then, the forming limit tests of AZ31B sheet at elevated temperatures are described in Sections 3 and 4 describes a further comparison that was done to evaluate the effectiveness of the theoretical FLD model. Subsequently, a numerical simulation of the warm forming process, based on the verified FLD prediction results, is given in Section 5. The numerical simulation results are explored and compared with the results of the warm forming experiment in Section 6. Conclusions are given in Section 7.

2 Theoretical computation of FLD

In this study, the M–K model was employed to predict the FLD of the AZ31B magnesium alloy sheet. Before describing the study, it is necessary to define a hardening law, a yield function, and a flow rule.

2.1 Hardening law description

The Fields–Backofen equation [25] was employed to investigate the plastic behavior of the AZ31B sheet. This equation indicates the relationship between the stress and the strain. The Fields–Backofen equation for most metal materials is given by:

$$\bar{\sigma} = K\bar{\varepsilon}^n \left(\frac{\dot{\bar{\varepsilon}}}{\dot{\bar{\varepsilon}}_0} \right)^m \tag{1}$$

where $\bar{\sigma}$ is the equivalent stress, K is the stress coefficient, $\bar{\varepsilon}$ is the equivalent strain, $\dot{\bar{\varepsilon}}$ is the strain rate, $\dot{\bar{\varepsilon}}_0$ is set as 1 s^{-1} to use the dimensionless strain rate. The work-hardening

phenomenon is expressed by the strain-hardening exponent n and the strain rate sensitivity exponent m . The parameters mentioned above can be obtained by using the equations as tabulated in Table 1 [26].

2.2 Logan–Hosford yield criterion

The Logan–Hosford yield criterion [27] is a function that is used to determine whether a material has carried out a plastic yielding under the action of stress. Under plain stress conditions, the Logan–Hosford yield criterion can be formulated by:

$$(1 + r)\bar{\sigma}^M = r(\sigma_1 - \sigma_2)^M + \sigma_1^M + \sigma_2^M \tag{2}$$

where M is the material exponent. For this study, the value of M was suggested as 6 [28]. r is the anisotropic coefficient of the AZ31B sheet; it can be obtained from uniaxial tensile tests [29]. Table 2 shows the values of the anisotropic coefficient under different temperatures when the angles between the tensile direction and rolling direction are 0° , 45° , and 90° . The normal anisotropy coefficient, r_n , is obtained from the Eq. (3). In this study, the value of r_n was adopted as the anisotropic coefficient for the theoretical analysis.

$$r_n = \frac{r_0 + 2r_{45} + r_{90}}{4} \tag{3}$$

2.3 Marciniak–Kuckzinsky model for formability prediction

The M–K model assumes that there is a narrow groove on the surface of a sheet metal (see Fig. 1). The strain localization is due to the presence of an imperfection. This appears in the zone of a material. The sheet specimen includes a safe zone and a groove zone which are shown as A and B . This groove causes a localized necking on the sheet metal. The initial groove is developed when proportional loading is applied outside the groove.

To model the groove, an imperfection factor, f_0 , is introduced which represents the sheet thickness ratio $f_0 = t_0^B/t_0^A$,

Table 1 Material characteristics of AZ31B magnesium alloy sheet

Elasticity	Plasticity
Young’s modulus, $E=44.5 \text{ GPa}$	Fields–Backofen equation, $\bar{\sigma}(\text{MPa}) = K\bar{\varepsilon}^n (\dot{\bar{\varepsilon}}/\dot{\bar{\varepsilon}}_0)^m$
Poisson’s ratio, $\nu=0.35$	$K(\text{MPa}) = \frac{3.24 \times 10^5}{t+273} - 406$, $t = \frac{T(^{\circ}\text{C})}{1(^{\circ}\text{C})}$
	$n = 0.016 \log(\dot{\bar{\varepsilon}}/\dot{\bar{\varepsilon}}_0) + \frac{62}{t+273} + 0.053$
	$m = \frac{-105}{t+273} + 0.303$

Table 2 Anisotropic coefficient of AZ31B sheet under different temperatures

Temperature (°C)	Anisotropic coefficient			
	r_0	r_{45}	r_{90}	r_n
200	1.29	1.87	1.52	1.64
250	0.82	1.29	1.11	1.13
300	0.63	0.83	0.82	0.78

where t_0^A and t_0^B are the initial thickness in the safety and groove region, respectively.

With respect to Fig. 1, we can formulate the force equilibrium in the 1 direction:

$$\sigma_{1A} \cdot t_A = \sigma_{1B} \cdot t_B \tag{4}$$

The compatibility requirement assumes that the elongation in the direction of the necking band is identical in both regions:

$$d\varepsilon_{2A} = d\varepsilon_{2B}. \tag{5}$$

Assuming that compatibility and equilibrium are satisfied in the groove region, the strain increment inside the groove $d\varepsilon_B$ is greater than that outside the groove $d\varepsilon_A$. Therefore, plain strain deformation occurs inside the groove, which causes the localization failure.

According to M–K theory, the basic equations for the M–K model in this study are expressed in the following:

1. The incompressibility in plastic forming:

$$d\varepsilon_1 + d\varepsilon_2 + d\varepsilon_3 = 0 \tag{6}$$

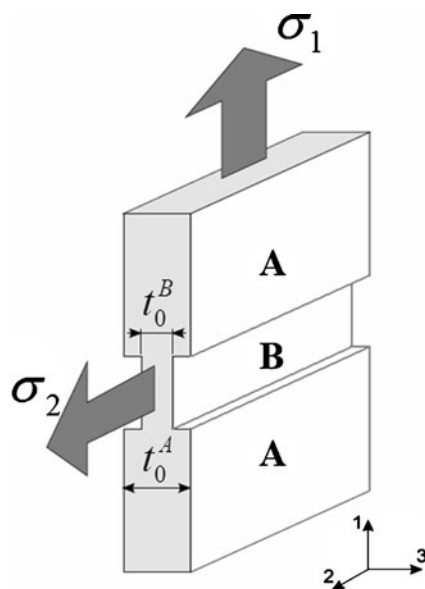


Fig. 1 Schematic diagram of M–K model

2. The condition of strain compatibility at the interface of areas A and B:

$$d\varepsilon_{2A} = d\varepsilon_{2B} = d\varepsilon_2 \tag{7}$$

3. The force equilibrium condition at the interface of areas A and B:

$$\sigma_{nn}^A t_A = \sigma_{nn}^B t_B, \quad \sigma_{nt}^A t_A = \sigma_{nt}^B t_B \tag{8}$$

where $\sigma_{nn}^A(\sigma_{nn}^B)$ and $\sigma_{nt}^A(\sigma_{nt}^B)$ are normal and tangential stress components at the interface of area A (B), respectively. $t_A(t_B)$ is real-time thickness of area A (B).

4. The J_2 deformation theory of plasticity:

$$d\varepsilon_i = dc \frac{\partial \bar{\sigma}}{\partial \sigma_i}, \quad i = 1, 2 \tag{9}$$

5. Defining several parameters as follows:

$$\varphi = \frac{\bar{\sigma}}{\sigma_1}; \quad \alpha = \frac{\sigma_2}{\sigma_1}; \quad \rho = \frac{d\varepsilon_2}{d\varepsilon_1}; \quad \beta = \frac{d\bar{\varepsilon}}{d\varepsilon_1} \tag{10}$$

where σ_1 and σ_2 are the major stress and the minor stress respectively. ε_1 and ε_2 are the major strain and minor strain respectively, $\bar{\sigma}$ is the equivalent stress and $\bar{\varepsilon}$ is the equivalent strain.

The iterative equation for calculation can be obtained based on the above basic formulae as well as the constitutive relation mentioned before.

$$\frac{1}{\varphi_A} (\bar{\varepsilon}_A + \Delta\bar{\varepsilon}_A)^{n(t)} \left(\frac{\beta_A}{\rho_A}\right)^{m(t)} \exp(\varepsilon_{3A}) = \frac{f_0}{\varphi_B} (\bar{\varepsilon}_B + \Delta\bar{\varepsilon}_B)^{n(t)} \left(\frac{\beta_B}{\rho_B}\right)^{m(t)} \exp(\varepsilon_{3B}) \tag{11}$$

where ε_3 is through-thickness strain and has the expression of $-(1+\beta)\varepsilon_1$, and during iteration $\Delta\varepsilon_{1B}$ is given to be 0.001 which can meet the requirement of computational precision [30].

From the Eqs. (2) and (10), we can obtain:

$$\varphi = \frac{\bar{\sigma}}{\sigma_1} = \left[\frac{1 + \alpha^M + r(1-\alpha)^M}{1+r} \right]^{\frac{1}{M}} \tag{12}$$

$$\rho = \frac{d\varepsilon_2}{d\varepsilon_1} = \frac{\alpha^{(M-1)} - r(1-\alpha)^{(M-1)}}{1+r(1-\alpha)^{(M-1)}} \tag{13}$$

The implemented solution strategy for this mixed boundary value problem can be solved with the iterative method of Eq. (11) [30]. The iterative flow chart used in the analysis is shown in Fig. 2.

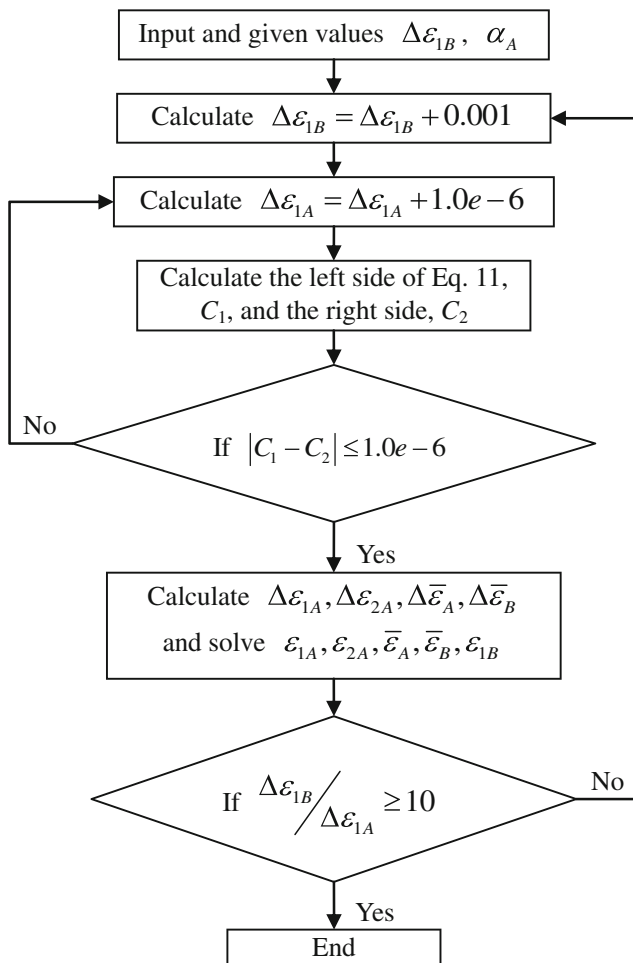


Fig. 2 The iterative flow chart of limit strains based on M–K theory

3 Forming limit tests of AZ31B sheet

A magnesium alloy sheet (AZ31B: Mg-3 %, Al-1 %, Zn) with 0.8 mm thickness and 18 μm average grain size was used for the forming limit tests. The widths of specimens ranging from 10 to 110 mm with laser marked grids were used in the test. In order to provide an isothermal condition during the test, a tailor-made die set with inner heaters [31] was employed in this study, as shown in Fig. 3. The heaters built in the die and punch were controlled

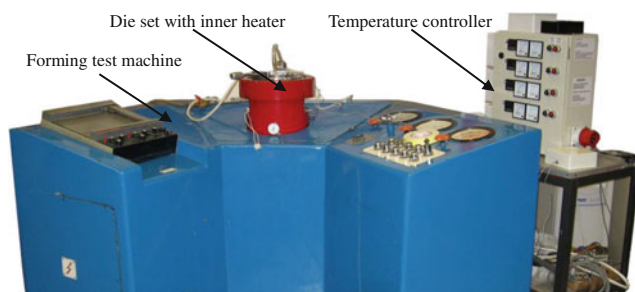


Fig. 3 Forming limit test machine with closed loop temperature controller [31]

by a temperature controller Omron E5CN. The controller was able to keep a stable temperature within $\pm 5^\circ$ through the temperature sensor installed in the tool [29]. The standard test method (ASTM E2218) was adopted to determine the FLD of the AZ31B sheet at the temperatures of 200, 250, and 300 $^\circ\text{C}$.

The deformed specimens are shown in Fig. 4. The test results were used for evaluating the FLDs of the AZ31B sheet. Three types of grids were measured to plot the experimental FLD, namely good, marginal, and cracked grids as shown in Fig. 4. The experimental method of acquiring the FLD is expensive and time consuming, so the experiments were performed at only one punch speed (1 mm/s) with elevated temperatures at 200, 250, and 300 $^\circ\text{C}$. The forming limit test results were compared with the theoretical results and to evaluate the correctness of the theoretical prediction.

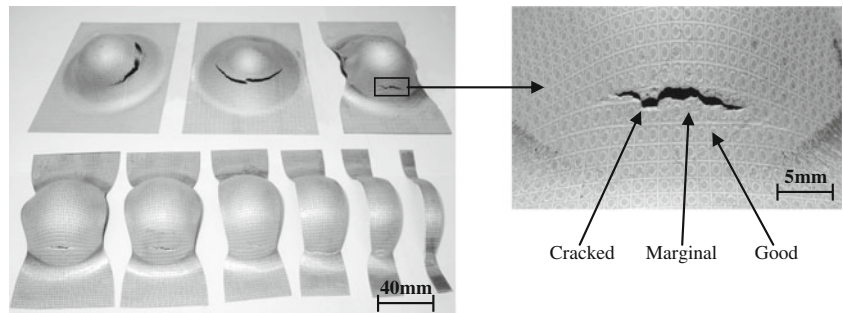
4 Comparison of FLDs from theoretical computation and experiment

In this section, the FLDs obtained from forming limit tests at different temperatures are compared with the theoretical ones. Although the strain rate was changing during each test [32], the effective plastic strain rate at the final stage of the tests was 0.01 s^{-1} when the punch speeds was 1 mm/s. Since the M–K model is sensitive to the initial imperfection factor f_0 , different values of f_0 (0.998, 0.995, and 0.990) were considered for the theoretical calculation and the proper value of f_0 was determined by comparing with the testing results.

Figure 5a–c show the comparison of the experimental and theoretical FLDs at different temperatures (200, 250, and 300 $^\circ\text{C}$). It can be seen from Fig. 5 that the values in the FLDs of the AZ31B sheet increase as the temperature increases, which means the formability of the AZ31B sheet can be improved at higher temperatures. The theoretical results show that the initial imperfection factor f_0 has a significant impact on the forming limits of the AZ31B sheets, a greater value of f_0 indicating that the defects in the sheet material are less obvious, thus enabling better formability of the material. By comparing the FLD results of experiments and theoretical predictions, it can be seen that the theoretical curves are most consistent with the forming limit test results when the f_0 is equal to 0.995. Therefore, the value of f_0 is given to be 0.995 in subsequent simulations.

So far, it is known that the magnesium alloy sheet possesses a strong rate sensitivity at high temperatures [5, 24, 32–34]. Therefore, the theoretical analysis of this study has been conducted on the effect of the strain rate on the FLDs of AZ31B sheet. Figure 6a–c show the FLDs obtained from M–K theory for three different strain rates at 200, 250, and 300 $^\circ\text{C}$. Comparing these results, it can be seen that the formability of the AZ31B sheet improves gradually as the strain rate decreases from 0.1 to 0.001 s^{-1} and the influence

Fig. 4 Specimens and types of grids for FLD measurement



of the strain rate on the FLDs becomes more significant with increasing temperatures, the increased effect of strain rate at high temperature can be explained by the increase of m value;

this is because the critical resolved shear stress decreases and the number of slip systems of the crystals increases with temperature rise, and the formability improves.

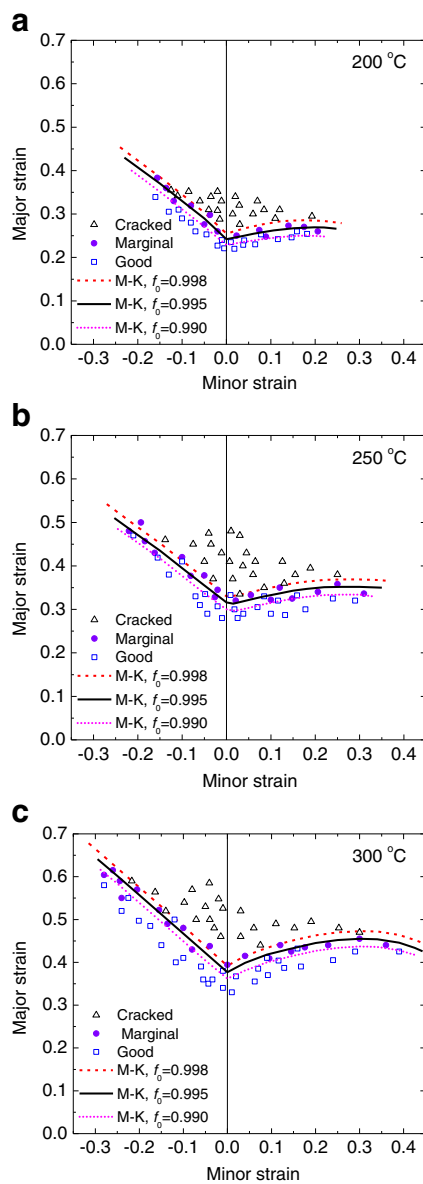


Fig. 5 Experimental and theoretical FLDs of AZ31B sheet at elevated temperatures

5 Numerical simulations for warm forming process

In this study, the commercial software package ABAQUS was employed for the numerical simulation to investigate the

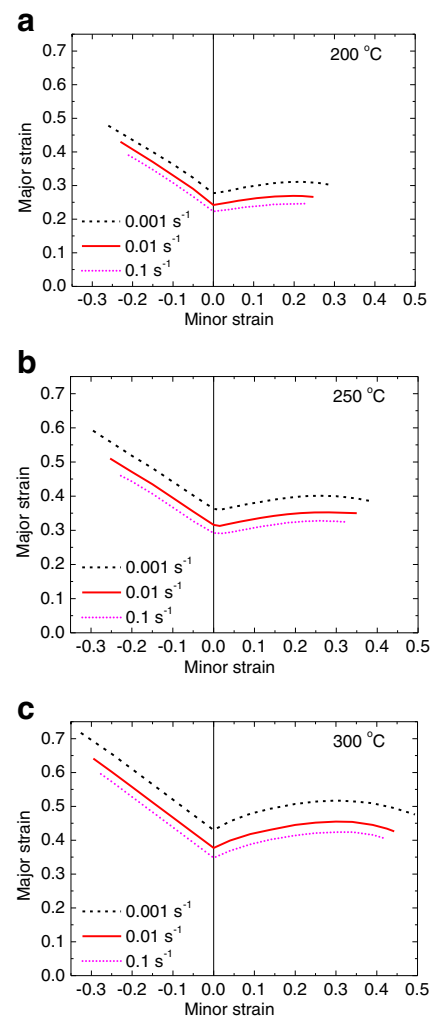


Fig. 6 The theoretical FLDs of AZ31B sheet at elevated temperatures



Fig. 7 3D model of the camera casing

formability of the magnesium alloy at elevated temperatures. A camera casing was used as an example for the numerical simulation as shown in Fig. 7. The 3D geometric models of the forming tool are shown in Fig. 8. During the simulation, the blank model was stamped and transformed into a box-shaped part (the final product), and the punch speed was set to be 1 mm/s. The size of the blank was 80×140 and 0.8 mm in thickness. AZ31B magnesium alloy sheets were selected as the material blanks. The sheet was modeled by shell elements (S4R) where five integration points had been used through the thickness. The interaction module between the tool and the blank was adopted as Coulomb friction, and the friction coefficient set as 0.25.

During the forming processes at the three specific elevated temperatures, the distributions of deformation speed of the camera casing were not uniform at different load steps due to the complex shape of the component. Therefore, in the FE simulation of the camera casing at a specific temperature (e.g., 250 °C), the strain rate of each element was determined from the quotient of the calculated strain value of an element divided by the increment of time step. With the input of FLCs obtained from three different strain rates, 0.001, 0.01, and 0.1 s⁻¹ (see Fig. 6) in the preprocess of the simulation, the forming limit values at various strain rates between 0.001 and 0.1 s⁻¹ were calculated using the interpolation method. Thus, FLCs could be used to identify fracture throughout the casing surface area with different strain rates at specific temperatures.

During the simulations, the variable *FLDCRT* was employed to analyze the formability of the component. The definition of *FLDCRT* is shown in Fig. 9. If the data points are

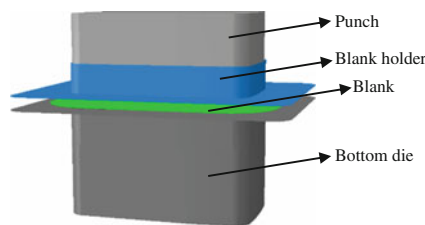


Fig. 8 3D model of forming tool

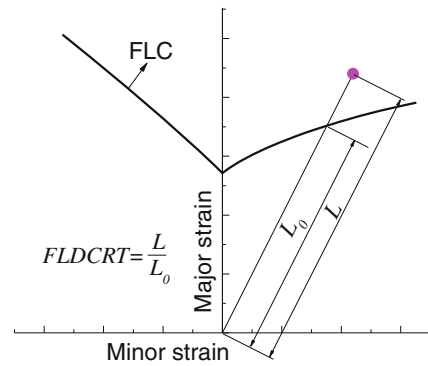


Fig. 9 Schematic diagram of the definition of *FLDCRT*

on or above the curve ($FLDCRT \geq 1$), a fracture will occur, and vice versa.

Figure 10a–c show the numerical simulation results for the camera casing at different temperatures. It can be seen clearly that the formability of the AZ31B sheet improved significantly as the temperature increased from 200 to 300 °C. In addition, the values of the *FLDCRT* at the corners are seen to be greater than the values in other regions, which means that

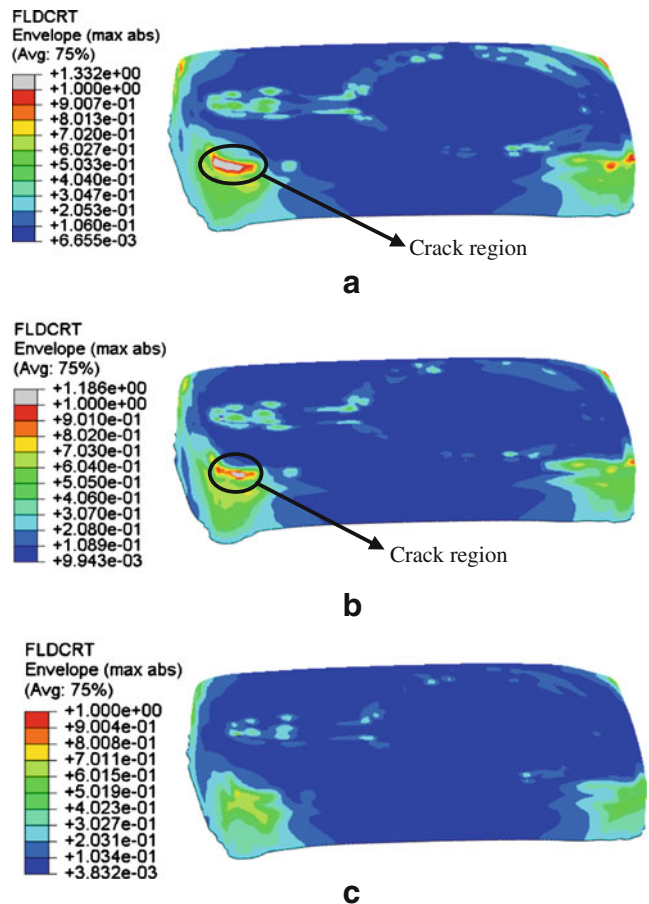


Fig. 10 The distribution of *FLDCRT* of a camera casing: a 200 °C, b 250 °C, c 300 °C

these corner regions may lead to cracking after a period of deformation. The simulation results show a big crack region at the lower left corner of the stamped product when the forming temperature was 200 °C. The crack region still appeared at the lower left corner when the forming temperature increased to 250 °C, but the area had decreased substantially. Finally, the crack region disappeared when the forming temperature increased to 300 °C.

The thickness distribution (STH) of the simulated camera casing at different punch strokes under selected temperatures of 200, 250, and 300 °C were shown in Figs. 11, 12, and 13, respectively. At the initial stage of the forming process, the thickness variation of the blank was small and even. When the punch stroke increased to 12 mm, the thickness reduction of the four corners, especially the lower left corner of the blank, became more obvious. Finally, the blank was formed into a camera casing (punch stroke=18 mm), and the thickness of the thinnest region (the lower left corner) decreased from 0.8 to 0.69 mm. Due to the complex shape and poor flowability, it was difficult to form the lower left corner, which indicates that this corner may crack during the forming.

The thickness variation shows a great influence on the formability of the warm forming component, i.e., the thicker the thickness, the greater the possibility of wrinkling; On the contrary, the likelihood of cracking is greater. As shown in Figs. 11, 12, and 13, the maximum value of the thickness

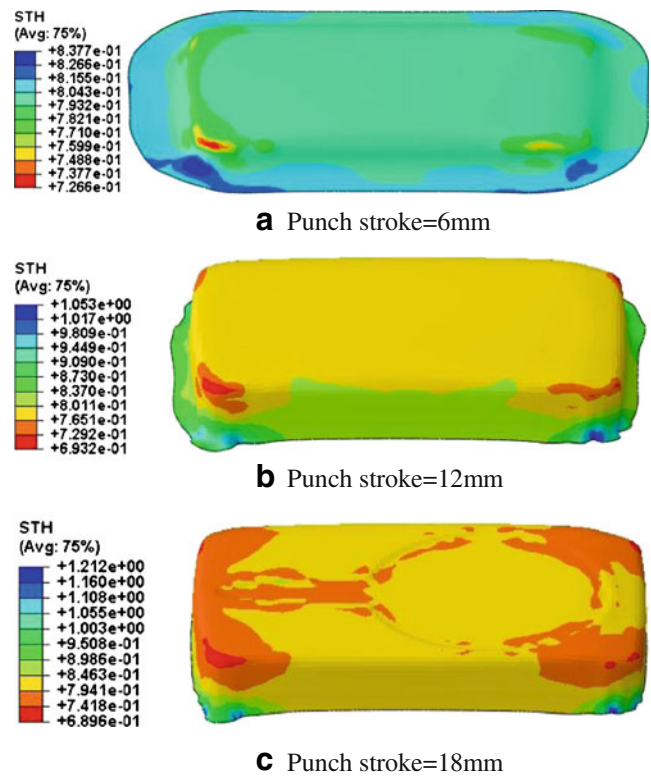


Fig. 12 The thickness distributions of the simulated camera casing at different punch strokes ($T=250\text{ }^{\circ}\text{C}$)

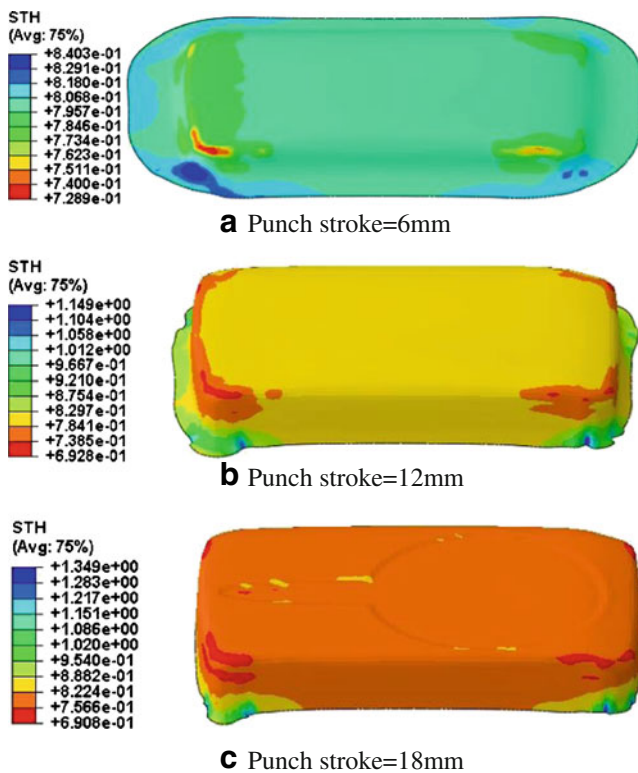


Fig. 11 The thickness distributions of the simulated camera casing at different punch strokes ($T=200\text{ }^{\circ}\text{C}$)

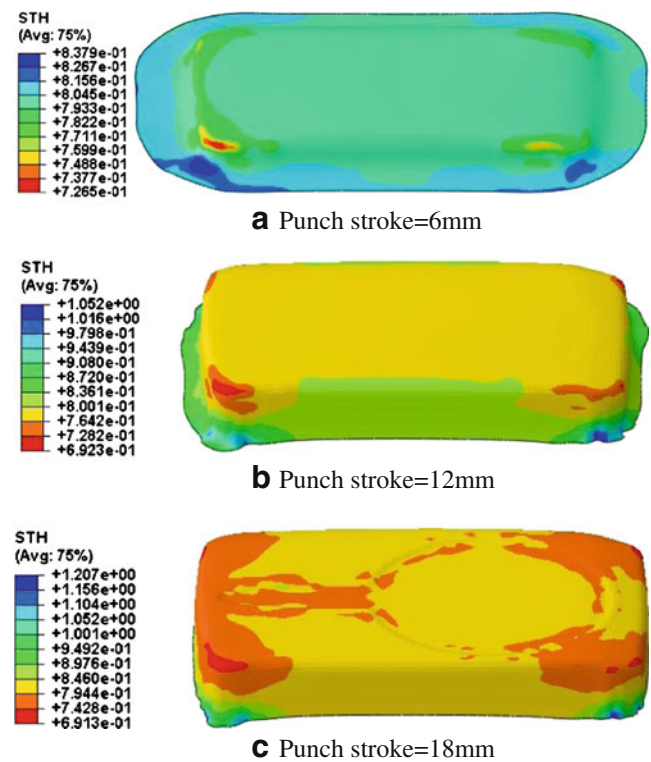


Fig. 13 The thickness distributions of the simulated camera casing at different punch strokes ($T=300\text{ }^{\circ}\text{C}$)



Fig. 14 160-Ton hydraulic press for carrying out warm forming experiment


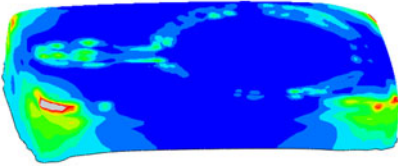

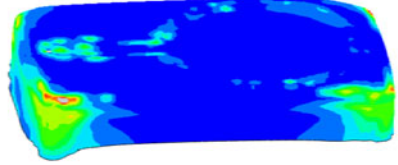

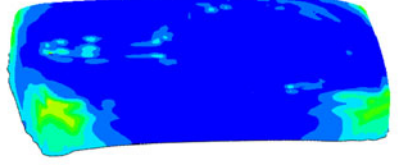
decreases significantly from 1.349 mm at 200 °C to 1.212 mm at 250 °C. Then the value experiences a slight decline, with the temperature increasing to 300 °C. Therefore, the possibility of wrinkling defects of the component can be reduced by increasing the forming temperature. Although the minimum value of the thickness keeps changing slightly when the forming temperature increases from 200 to 300 °C, the cracking defects of the component tend to decrease due to the better flowability of magnesium alloy at higher temperatures.

6 Comparison between numerical and experimental of warm forming results

To verify the results generated from the numerical simulations, a corresponding warm forming experiment was carried out in this study. The warm forming experimental apparatus employed is shown in Fig. 14. The material used in this study was a commercial AZ31B magnesium alloy sheet with 0.8 mm in thickness. The punch and the die were heated to elevated temperatures by cartridge heaters, and the punch speed was 1 mm/s during the forming process. The blank at room temperature was sandwiched between the high temperature tools and it was detected at temperatures of approximately 200, 250, and 300 °C.

A comparison between the experimental results and the predicted results from the numerical simulation is shown in Table 3. The simulation results show that the cracking appeared at the lower left corner of the components when the forming temperatures were 200 and 250 °C. There was a corresponding cracking appearing at approximately the same location in the experimental results, but the crack regions were larger than those of the simulation results. This is because the theoretical analysis in this paper only considered the crack initiation in the necking zone without considering the crack propagation, while the crack region of the experimental test was the final result after crack propagation. Both the numerical simulation and the experimental results show that we can get qualified (no cracking) forming products when the forming temperature reaches 300 °C.

Table 3 Comparison between numerical and experimental results of the specimens

Temperature (°C)	Experimental results	Numerical simulated results
200		
250		
300		

7 Conclusions

In this paper, a theoretical method has been proposed for predicting the formability of AZ31B sheets at elevated temperatures by combining the M–K model with the Logan–Hosford yield criterion. By comparing the theoretical analysis, numerical simulations and experimental results, the following conclusions were obtained:

1. The forming limits of the AZ31B magnesium alloy sheet increase with temperature rise and with strain rate decrease. In addition, the influence of strain rate on the FLDs becomes more significant with increasing temperatures, the increased effect of strain rate at high temperature can be explained by the increase of m value; this is because the critical resolved shear stress decreases and the number of slip systems of the crystals increases with temperature rise, thus the formability improves. Both the numerical simulations and warm forming experiments show that the qualified (no cracking) products can be obtained when the forming temperature reaches 300 °C.
2. The results of the numerical simulation show a good agreement with the results of the warm forming experiment in terms of the crack location and whether cracking appears or not under different temperatures. Therefore, the proposed theoretical method is valid for the warm forming process of magnesium alloy sheets.

Acknowledgments The work described in this paper was partially supported by grants from the Research Grant Council of the Hong Kong Special Administrative Region, China (project nos. PolyU 511511, 511909, and G-YJ11).

References

1. Fredrich H, Schumann S (2001) Research for a new age of magnesium in the automotive industry. *J Mater Process Technol* 117:276–281
2. Mustafa KK (2008) Magnesium and its alloys applications in automotive industry. *Int J Adv Manuf Technol* 39:851–865
3. Yoshinaga H, Horiuchi R (1963) On the flow stress of α solid solution Mg–Li alloy single crystals. *Trans JIM* 4:134–141
4. Kaneko J, Sugamata M, Numa M, Nishikawa Y, Takada H (2000) Effect of texture on the mechanical properties and formability of magnesium wrought materials. *J Jpn Inst Met* 64(2):141–147
5. Liu ZG, Lasne P, Massoni E (2011) Formability study of magnesium alloy AZ31B. In: AIP Conference Proceedings. Seoul, Republic of Korea, pp 150–157
6. Aida S, Tanabe H, Sugai H, Takano I, Ohnuki H, Kobayashi M (2000) Deep-drawability of cup on AZ31 magnesium alloy plate. *J Jpn Inst Light Met* 50:456–461
7. Zhang H, Huang GS, Kong DQ, Sang GF, Song B (2011) Influence of initial texture on formability of AZ31B magnesium alloy sheets at different temperatures. *J Mater Process Technol* 211:1575–1580
8. Kohzu M, Yoshida F, Higashi K (2003) Evaluation of press formability in magnesium alloy. *Mater Sci Forum* 419–422:321–326
9. Lee S, Chen YH, Wang JY (2002) Isothermal sheet formability of magnesium alloy AZ31 and AZ61. *J Mater Process Technol* 124:19–24
10. Lin YL, He ZB, Yuan SJ, Wu J (2011) Formability determination of AZ31B tube for IHPF process at elevated temperature. *Trans Nonferrous Met Soc China* 21:851–856
11. Yoshihara S, Yamamoto H, Manabe K, Nishimura H (2003) Formability enhancement in magnesium alloy deep drawing by local heating and cooling technique. *J Mater Process Technol* 143: 612–615
12. Palaniswamy H, Ngaile G, Altan T (2004) Finite element simulation of magnesium alloy sheets forming at elevated temperatures. *J Mater Process Technol* 146:52–60
13. Abu-Farha F, Verma R, Hector LG (2012) High temperature composite forming limit diagrams of four magnesium AZ31B sheets obtained by pneumatic stretching. *J Mater Process Technol* 212: 1414–1429
14. Keeler SP, Backofen WA (1963) Plastic instability and fracture in sheets stretched over rigid punches. *ASM TRANS Q* 56:25–48
15. Ozturk F, Lee D (2004) Analysis of forming limits using ductile fracture criteria. *J Mater Process Technol* 147:397–404
16. Swift HW (1952) Plastic instability under plane stress. *J Mech Phys Solids* 1:1–18
17. Hill R (1952) On discontinuous plastic states, with special reference to localized necking in thin sheets. *J Mech Phys Solids* 1:19–30
18. Marciniak Z, Kuckzinsky K (1967) Limit strain in the processes of stretch-forming sheet metal. *Int J Mech Sci* 9:609–620
19. Hutchinson JW, Neale KW (1979) Sheet necking-II. Time-independent behaviour. In: Koistinen DP, Wang NM (eds) *Mechanics of sheet metal forming*. Springer, New York, pp 127–153
20. Parmar A, Mellor PB (1978) Prediction of limit strains in sheet metal using a more general yield criterion. *Int J Mech Sci* 20:385–391
21. Hill R (1979) Theoretical plasticity of textured aggregates. *Math Proc Camb Philos Soc* 85:179–191
22. Ferron G, Mliha Touati M (1985) Determination of the forming limits in planar-isotropic and temperature-sensitive sheet metals. *Int J Mech Sci* 27:121–133
23. Min JY, Lin JP, Li JY, Bao WH (2010) Investigation on hot forming limits of high strength steel 22MnB5. *Comput Mater Sci* 49:326–332
24. Naka T, Uemori T, Hino R, Kohzu M, Higashi K, Yoshida F (2008) Effects of strain rate, temperature and sheet thickness on yield locus of AZ31 magnesium alloy sheet. *J Mater Process Technol* 201: 395–400
25. Fields DS, Backofen WA (1957) Determination of strain hardening characteristics by torsion testing. *Proc ASTM* 57:1259–1272
26. Takuda H, Morishita T, Kinoshita T, Shirakawa N (2005) Modeling of formula for flow stress of a magnesium alloy AZ31 sheet at elevated temperatures. *J Mater Process Technol* 164–165:1258–1262
27. Cazacu O, Plunkett B, Barlat F (2006) Orthotropic yield criterion for hexagonal closed packed metals. *Int J Plast* 22:1171–1194
28. Logan RW, Hosford WF (1980) Upper-bound anisotropic yield locus calculations assuming $\langle 111 \rangle$ -pencil glide. *Int J Mech Sci* 22:419–430
29. Wang L, Chan LC, Lee TC (2008) Formability analysis of magnesium alloy sheets at elevated temperatures with experimental and numerical method. *J Manuf Sci Eng-Trans ASME* 130:61003(7)
30. Graf A, Hosford WF (1990) Calculations of forming limit diagrams. *Metallurgical Transactions A* 21:87–94
31. Lai CP, Chan LC, Chow CL (2007) Effects of tooling temperatures on formability of titanium TWBs at elevated temperatures. *J Mater Process Technol* 191:157–160
32. Naka T, Torikai G, Hino R, Yoshida F (2001) The effects of temperature and forming speed on the forming limit diagram for type 5083 aluminum–magnesium alloy sheet. *J Mater Process Technol* 113: 648–653
33. Palumbo G, Sorgente D, Tricarico L (2008) The design of a formability test in warm conditions for an AZ31 magnesium alloy avoiding friction and strain rate effects. *Int J Mach Tools Manuf* 48: 1535–1545

34. Xu JR, Yu HP, Li CF (2012) Effects of process parameters on electromagnetic forming of AZ31 magnesium alloy sheets at room temperature. *Int J Adv Manuf Technol* 66:1–12

Partial information of this paper was published in the proceedings of “2013 2nd International Conference on Micro Nano Devices, Structure and Computing Systems (MNDSCS 2013)”.